How to cite: *Angew. Chem. Int. Ed.* **2025**, *64*, e202509549
doi.org/10.1002/anie.202509549

Photoredox Catalysis

Tertiary Phosphine Diversification via Photochemical P—C Chemoselective Cleavage of Phosphonium Salts

Ziyu Gan[+], Jiajin Chen[+], Hailong He[+], Yun-Yi Zhao, Zhiyan Xue, Ziyang Chen, Lifang Wang, Shuyang Liu, Hao Wang, Hua Fu, and Yunhe Jin**

Abstract: Differentially substituted phosphines are indispensable in medicines, materials, and catalysis, yet their customizable synthesis, traditionally depending on unstable P—H/halogen reagents, remains formidably challenging. Here, we report a photoredox strategy enabling controllable aryl substitution through chemoselective P—C cleavage. By engineering electron donor-acceptor complexes between phosphonium salts and tertiary amines, this metal-free protocol realizes three consecutive hydrocarbyl exchanges for delivering tri-diverse-aryl phosphines with transition metal contamination elimination and broad functional group tolerance including unprotected amines and hydroxyls, facilitating late-stage modification of drugs/commercial ligands and construction of P,O,S-tridentate architectures and chiral P-stereogenic centers. Mechanistic studies reveal the dynamic pentacoordinated-phosphorane-complex formation nature and the radical-intermediate pathway, while the chemoselectivity originates from different P—C bond strengths. This work establishes a modular and sustainable platform for programming-level precision phosphine engineering.

Introduction

Phosphines with differentiated substitution patterns serve as cornerstone motifs across modern chemistry, driving advancements in materials science,[1] medicinal discovery,[2–4] and organic light-emitting diodes (OLEDs).[5] Importantly, their preeminence in coordination chemistry stems from intrinsically tunable electronic and steric profiles, which dictate catalytic performance in transition metal complexes.[6–15] Seminal contributions by Buchwald,[6,7] Zhou,[16] and so on—demonstrating phosphine ligands' unparalleled efficacy in C—N cross-coupling and asymmetric hydrogenation—epitomize their indispensable role in catalytic innovation. These organometallic systems exhibit disparate catalytic behaviors depending on phosphine architecture, where subtle substituent modifications dramatically modulate reactivity and selectivity through electronic perturbation and spatial confinement. Such structure-activity relationships underscore the critical need for modular synthetic strategies to access phosphines with customizable substitution patterns—a capability paramount to systematic ligand engineering and reaction optimization.[8]

Despite their fundamental importance, the synthetic accessibility of triarylphosphines remains disproportionately limited compared to their utility. This disparity originates from two inherent challenges: i) the oxidative instability of trivalent phosphorus centers and ii) the synthetic complexity of achieving sequential aryl substitutions. While triarylphosphines demonstrate improved air stability and broader applicability, existing synthetic paradigms face several critical limitations.

Current methodologies mainly include i) transition metal-catalyzed cross-couplings between phosphanes and aryl halides,[17,18] ii) nucleophilic substitutions using Grignard/lithium reagents,[19] iii) radical-mediated stannylative arylations,[20] and iv) reductive deoxygenation of phosphine oxides.[21–24] However, these approaches predominantly enable single aryl group installation while struggling to achieve iterative diversification.

The strategic construction of tri-diverse-aryl-substituted trivalent phosphines presents a formidable synthetic challenge, with four principal pathways theoretically available (Figure 1a, Routes A-D). Route A initiates with $PhPCl_2$ arylation via Grignard reagents, requiring meticulous protecting group orchestration to prevent over-substitution.[25] Route B employs transition metal-catalyzed iterative cross-coupling, which achieves chemoselectivity at the expense of stoichiometric excess and strict cryogenic conditions to suppress multi-substituted byproducts.[26] $POCl_3$-derived sequential nucleophilic substitutions (Route C) theoretically permit customizable aryl introduction, but still suffer from intractable

[*] Z. Gan[+], J. Chen[+], H. He[+], Z. Xue, Z. Chen, L. Wang, S. Liu, Prof. Y. Jin
State Key Laboratory of Fine Chemicals, School of Chemistry, Dalian University of Technology, Dalian 116024, China
E-mail: jinyh18@dlut.edu.cn

Prof. H. Fu
Key Laboratory of Bioorganic Phosphorus Chemistry and Chemical Biology, Department of Chemistry.Tsinghua University, Beijing 100084, China
E-mail: fuhua@mail.tsinghua.edu.cn

Y.-Y. Zhao, Prof. H. Wang
State Key Laboratory and Institute of Elemento-Organic Chemistry, College of Chemistry and Frontiers, Science Center for New Organic Matter, Nankai University, Tianjin 300071, China

[+] These authors contributed equally to this work.

Additional supporting information can be found online in the Supporting Information section

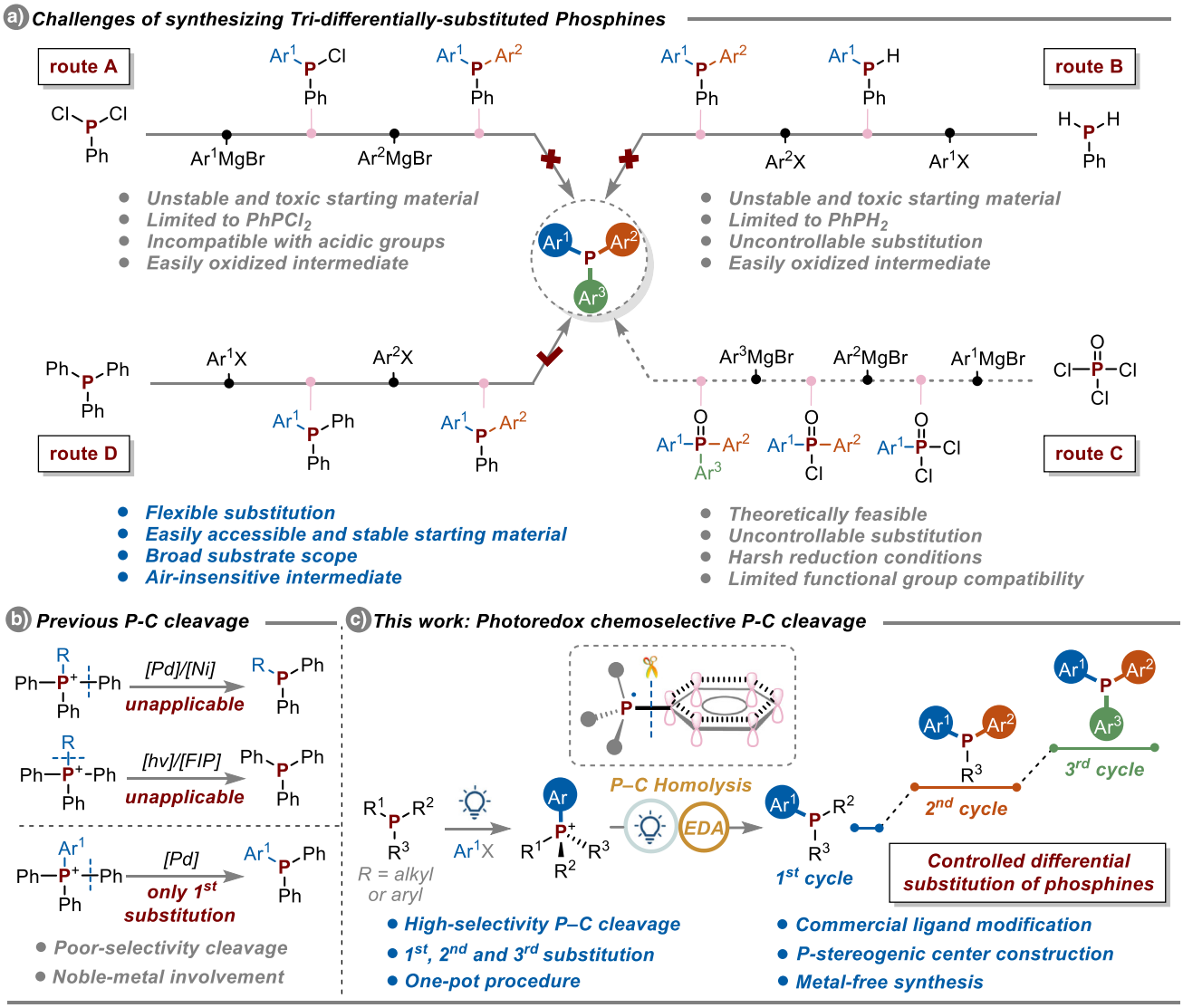

Figure 1. Progress toward tri-differentially-substituted phosphine synthesis. a) Challenges of synthesizing tri-differentially substituted phosphines. b) Previous P—C bond cleavage. c) Photoredox chemoselective P—C bond cleavage.

selectivity and over-reaction issues during multi-step transformations. Subsequent reduction of P(V) intermediates to P(III) species introduces additional constraints,[21–24] as overly harsh reductive conditions prove incompatible with sensitive functionalities prevalent in drug intermediates. These convergent limitations—spanning safety risks, step inefficiency, and narrow functional group tolerance—collectively demarcate the frontier for next-generation phosphine synthesis technologies capable of customizable, iterative aryl installation under ambient conditions.

An emerging paradigm centers on valence cycling between tertiary phosphines and quaternary phosphonium salts (Route D),[27–29] capitalizing on the dynamic P—C bond reorganization observed in catalytic systems. Intriguingly, the inherent ligand-metal exchange phenomenon has been repurposed as a strategic lever for rapid ligand diversification.[30] This conceptual inversion finds experimental validation in Morandi's nickel-catalyzed dearylation of alkyl/aryl-phosphonium salts[28] and Wang's analogous palladium-mediated system[29] (Figure 1b). While these breakthroughs enable alkyl-for-aryl substitution, their applicability remains confined to aliphatic group installation. Parallel developments in radical chemistry reveal phosphonium salts' untapped potential as sp^3-carbon radical reservoirs.[31–33] Chen's seminal photochemical platform[31,32] and Morandi's frustrated ion pair (FIP) strategy[33] exemplify single-electron transfer (SET)-mediated $C(sp^3)$—$C(sp^3)$ bond formation, albeit at the cost of phosphine expenditure as sacrificial leaving groups—a critical limitation that plagues atom economy. More fundamentally, none of these approaches address the core challenge of iterative aryl substitution at phosphorus. Early attempts to circumvent this barrier through tetraarylphosphonium intermediates met limited success. Chan's pioneering Pd-catalyzed phosphination (2000)[34,35] and Morandi's reversible $C(sp^2)$–P metathesis (2017)[27] achieved single aryl substitution, yet inherent electronic similarity among aryl C—P bonds

engenders poor chemocontrol. This mechanistic bottleneck manifests in complex product mixtures requiring tedious chromatographic separation, with viable yields attainable only for one-time substitution.

Critical analysis of existing Route D reveals two persistent synthetic barriers that preclude customizable aryl diversification: i) Precision phosphonium salt formation; ii) Chemoselective P─C scission. Recently, our group introduced a photochemical platform that addresses the first challenge of tetraarylphosphonium intermediate construction through electron donor-acceptor (EDA) complex engineering.[36] Building upon this foundation and our extensive expertise in catalyst-free photosynthesis[36–38] and phosphorus chemistry,[39,40] we herein engineered a pentacoordinated-phosphorane EDA complex system to achieve chemoselective P─C bond cleavage (Figure 1c). The subtle electronic interplay between phosphorus-centered radicals and aryl substituents—modulated by substituent electronic nature—enables remarkable bond dissociation selectivity under mild photoredox conditions. This breakthrough permits metal-free, one-pot aryl exchange on tertiary phosphines with precise chemocontrol. Through iterative implementation, this protocol accomplishes three consecutive aryl substitutions in a modular fashion, yielding tri-diverse-aryl phosphines with customizable architectures. The advantages and technical merits including step economy and operational simplicity are further amplified by demonstrated wide applications in gram-scale synthesis, post-modification of commercial ligands, and construction of P-stereogenic centers.

Results and Discussion

Synthesized by our just-established metal-free phosphonium salt construction protocol,[36] compound **2a** was systematically subjected to parametric optimization (Table 1). Initial reductant screening (entries 1–4) revealed diisopropylethylamine (DIPEA) as optimal, delivering **3a** in 73% yield (vs. ≤61% for Hantzsch ester/NEt_3/tetramethylethylenediamine). Subsequent single solvent evaluation (entries 4–8) identified DMA (dimethylacetamide) as a suitable media, outperforming aprotic solvents (CH_3CN: 30%; dimethylformamide (DMF): 36%) and halocarbons (CH_2Cl_2: <5%). Further addition of some water presented DMA/H_2O (9:1 v/v) to be a better choice (91% yield, entry 9). Different types of mixed solvent systems were attempted next, but none performed better (entries 10–14). The positive impact of water may be attributed to its ability to enhance the dissociation of phosphonium salt anions and thus facilitate the formation of the EDA complex. Photon wavelength studies (entries 15,16) confirmed 405 nm irradiation as critical for efficient activation (ΔYield: +28% vs. 455 nm). Control experiments (entries 17,18) established dual dependence on both light irradiation and inert atmosphere (N_2), with the omission of either parameter causing complete reaction arrest.

With optimized conditions established, systematic substrate scope evaluation was conducted to delineate functional group tolerance across diverse architectures (Figure 2). Hydroxyl-containing moieties, including phenolic groups (**3b**, 88%) and benzyl alcohols at *meta*- (**3c**, 82%) or *para*-positions (**3d**, 87%) remain intact without protective strategies, while heterocyclic substrates—from oxygen-containing aliphatic (**3e**, **3f**) and aromatic cycles (**3g**) to sulfur-embedded benzothiophenes (**3i**, **3j**) and nitrogenous indoles (**3v**, **3w**)—exhibit robust compatibility (65%–88%). Notably, anisole thioether—a known catalyst poison in transition metal systems—proved compatible, delivering **3h** in 88% yield. Pharmacophoric elements critical to drug activity, such as fluorine (**3l**, **3t**), trifluoromethyl (**3m**, **3u**), and trifluoromethoxy (**3q**) groups, are seamlessly incorporated in good yields. The protocol's capacity for unprotected amine incorporation was evidenced by **3n** (80% yield), and the methodology further enables dual functionalized aryls as demonstrated by amino/various other groups-hybrid arenes (**3p**–**3u**). Moreover, commercial triarylphosphines instead of triphenylphosphine serve as viable substrates as well, affording diversified products (**3x**–**3z**, 77%–85%) with retained efficiency, and late-stage modification of pharmaceuticals—including anti-inflammatory and analgesic *Ibuprofen* (**3aa**, 84%) and *Naproxen* (**3ab**, 73%)—proceeds smoothly. Crucially, the directinstallation of unprotected nucleophiles (-NH_2, -OH) eliminates tedious protection-deprotection sequences, underscoring the protocol's versatility in complex phosphine engineering. Furthermore, the chemoselectivity of the reaction was investigated through a ratio analysis on several typical products with a ^{31}P NMR spectrum of the crude product (Figures S11–S14). According to the results, the phosphonium salts were almost completely consumed,

Table 1: Optimization of the reaction conditions.[a]

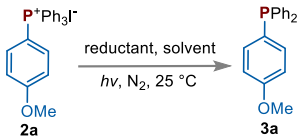

2a **3a**

Entry	Reductant	Solvent	Wavelength	Yield (%)[b]
1[c]	HE	DMA	405 nm	58
2	NEt_3	DMA	405 nm	61
3[d]	TMEDA	DMA	405 nm	53
4	DIPEA	DMA	405 nm	73
5	DIPEA	DMF	405 nm	36
6	DIPEA	CH_3CN	405 nm	30
7	DIPEA	CH_2Cl_2	405 nm	trace
8	DIPEA	MeOH	405 nm	22
9	DIPEA	DMA:H_2O (9:1)	405 nm	91
10	DIPEA	DMA:MeOH (9:1)	405 nm	42
11	DIPEA	DMA:EtOH (9:1)	405 nm	35
12	DIPEA	DMA:*i*-PrOH (9:1)	405 nm	40
13	DIPEA	DMA:DCM (9:1)	405 nm	trace
14	DIPEA	DMA:CH_3CN (9:1)	405 nm	31
15	DIPEA	DMA:H_2O (9:1)	455 nm	63
16	DIPEA	DMA:H_2O (9:1)	365 nm	91
17	DIPEA	DMA:H_2O (9:1)	dark	0
18[e]	DIPEA	DMA:H_2O (9:1)	405 nm	16

[a] Reaction conditions: **2a** (0.2 mmol), reductant (1 mmol, 5 eq), solvent (2.0 mL) under N_2 and irradiation of 30 W LEDs for 24 h. [b] Isolated yield. [c] HE = Hantzsch ester. [d] TMEDA = tetramethylethylenediamine. [e] Air atmosphere.

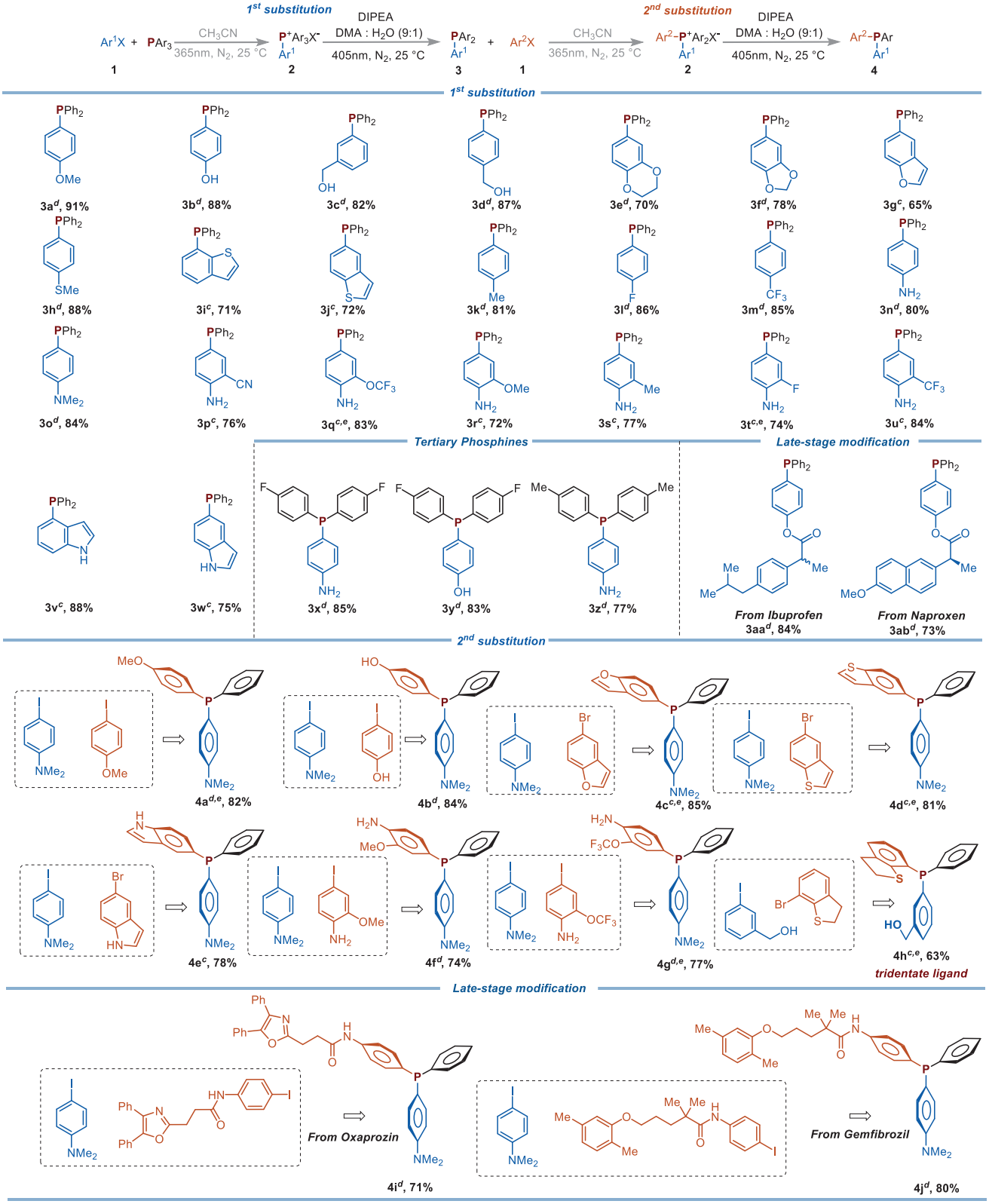

Figure 2. Substrate scope for arylphosphonium salts[a,b]. [a] Reaction conditions: **2** (0.2 mmol), DIPEA (1 mmol, 5 equiv.), DMA:H_2O (9:1) (2.0 mL) under N_2 and 30 W 405 nm LED irradiation for 24 h. [b] Isolated yield. [c] $X^- = Br^-$. [d] $X^- = I^-$. [e] Isolated as borane complex.

and the selectivities were proved to be high enough (25:1) for products with over 85% yields (**3l**, **3m**). However, for the products with moderate yields (**3g**, **3r**, 65%–72%), the reactions provided the target product along with varying proportions of byproducts. The ratios of the products **3g** and **3r** to the byproduct triphenylphosphine were 3.2:1 and 5.6:1, respectively. These outcomes conform to our initial conjecture that the relatively low yields are mainly due to reduced selectivity.

Building upon the success of primary aryl substitution, we systematically investigated second-stage diversification using **3o** as a typical starting material. Elaborately designed reaction conditions enabled chemoselective displacement of the secondary phenyl group with methoxy- (**4a**, 82%) or hydroxyl-substituted arenes (**4b**, 84%), establishing tri-diverse-aryl phosphines through sequential functionalization. Heterocyclic architectures—including benzofuran (**4c**, 85%), benzothiophene (**4d**, 81%), and indole derivatives (**4e**, 78%)—maintained structural integrity while acquiring potential multi-dentate coordination capabilities during the transformation. The protocol further demonstrated double-functionalization arenes with amino/methoxy (**4f**, 74%) and amino/trifluoromethoxy groups (**4g**, 77%) as the second arylation candidates. Impressively, iterative application to bidentate precursor **3c** yielded a P,O,S-tridentate ligand (**4h**)—a previously inaccessible coordination architecture. Pharmaceutical relevance was underscored through late-stage diversification of *Oxaprozin* (**4i**, 71%) and *Gemfibrozil* (**4j**, 80%), showcasing precise installation of phosphine motifs onto complex drug scaffolds to extend native functionalities.

Despite the remarkable success we achieved in the aforementioned aromatic substitution strategy using triarylphosphines as the substrates, the observed chemoselectivity profile reveals, however, a strong electronic dependence: tetraarylphosphonium salts undergo preferential excision of electron-deficient aryl groups, fundamentally limiting the systems to electron-rich aryl installations. To transcend this electronic constraint, strategic substrate engineering employing trialkylphosphines enables electron-deficient aryl incorporation via selective C(sp^3)–P cleavage (Figure 3). The functional-group compatibility investigation uncovered cyclohexyl's exceptional leaving group aptitude (**5b–5j**), achieving selective removal even with electron-poor aryl partners (**5b–5e**, 65%–82%). Expanding the leaving group scope, we next evaluated n-butyl's performance, achieving viable access to **5k–5m** with practical yields. The ratios of the selected products **5e** and **5l** to the byproduct trialkylphosphine were also detected to be 4:1 and 3.1:1, respectively, further demonstrating that the reduced selectivity is primarily responsible for the low yield (Figures S16, S18). Subsequently, secondary substitution studies of **5a** were conducted. By introducing electron-withdrawing group esters and cyanides to the *ortho-*, *meta-*, and *para*-positions of the second arylation reagents, we observed that these functionalized aryl groups remained well-incorporated, resulting in efficient synthesis of **6a** to **6f** with yields ranging from 60% to 84%. Strikingly, pyridine—a potent metal-coordinating heterocycle—is smoothly incorporated (**6g**, 67%), exemplifying the protocol's proficiency in constructing polydentate architectures.

The synthetic versatility of our methodology is further demonstrated through advanced applications in phosphine engineering and ligand post-modification (Figure 4). By integrating phosphonium salt formation with subsequent P─C bond cleavage into a two-step one-pot protocol, we successfully simplify operations by eliminating intermediate purification steps, thereby reducing product loss and enhancing efficiency through continuous reaction progression. Customizable application of this streamlined approach enabled the first synthesis of tri-controllable phosphine **7** from triphenylphosphine through three consecutive cycles (26% overall yield, Figure 4a), establishing a new paradigm for modular phosphorus chemistry. The practical utility is further evidenced by precision modification of commercially available ligands which are widely employed in Buchwald C─N coupling and Suzuki C─C coupling reactions: anisole installation on CyJohnPhos (**8**, 65%, Figure 4b) and dibenzothiophene incorporation into XantPhos (**9**, 53%, Figure 4c) proceed efficiently without compromising catalytic cores. This transformative strategy not only significantly diversifies the accessible ligand chemical space but also enables expedited generation of tailored phosphine architectures through modular functionalization, thereby establishing a robust platform for next-generation catalyst design and discovery. Moreover, using a stereochemically-pure aryl-substituted phosphonium salt, we successfully synthesized chiral valine-derived phosphine **10** (44% four-step yield, dr $\geq$ 20:1, Figure 4d) whose configurational isomers are readily separable—a significant advantage for potential application in asymmetric catalysis. Crucially, the entire ligand construction process operates under a transition metal-independent regime at ambient temperature, completely circumventing the persistent challenge of residual palladium/nickel contamination inherent to traditional metal-catalyzed phosphine syntheses, thereby eliminating false-positive-result risks in downstream catalytic applications and meeting stringent requirements for therapeutic molecule synthesis. Encouragingly, scalability is confirmed through continuous-flow implementation with a custom-designed reactor (Figure 4e), delivering gram-scale **3o** (1.16 g, 76%) with retained efficiency, thereby bridging laboratory innovation to industrial applicability.

To elucidate the molecular origin of the exceptional chemoselectivity in P─C bond cleavage, we undertook comprehensive mechanistic studies integrating photochemical, spectroscopic, spin-trapping, and computational techniques (Figure 5). Initial light-switching experiments revealed strict photo-dependence: alternating 2-h dark/light cycles caused immediate reaction arrest upon irradiation cessation (conversion <1%) and rapid resumption upon re-illumination (Figure S1). This discontinuous progression profile conclusively excludes radical chain propagation mechanisms while confirming photon-driven initiation. UV-vis spectral monitoring of the **2a**/DIPEA system unveiled critical insights into electron donor-acceptor (EDA) complex dynamics. While pure **2a** showed negligible absorption at 405 nm (absorbance $A < 0.1$ a.u.), incremental DIPEA addition (0→5 equiv) induced progressive bathochromic shifts ($\Delta A > +1.1$ a.u. at 405 nm), accompanied by solution darkening from colorless to deep yellow (Figure 5a). Subsequent 405 nm irradiation

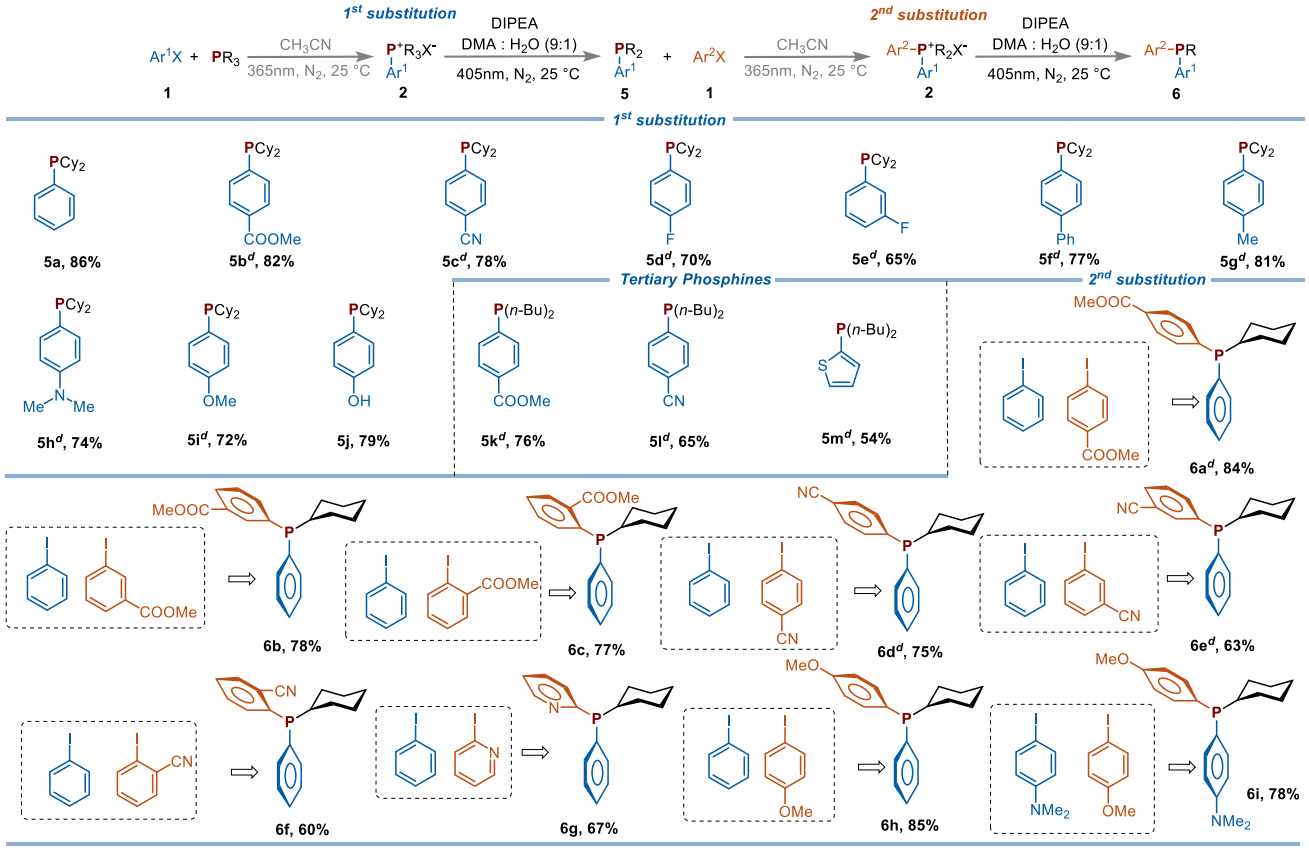

Figure 3. Substrate scope for alkylphosphonium salts[a–c]. [a] Reaction conditions: **2** (0.2 mmol), DIPEA (1 mmol, 5 equiv.), DMA:H_2O (9:1) (2.0 mL) under N_2 and 30 W 405 nm LED irradiation for 24 h. [b] Isolated yield. [c] $X^- = I^-$. [d] Isolated as borane complex.

triggered hypsochromic reversion with complete visible-range absorption extinction after 24 h, directly visualizing SET-induced EDA dissociation.

Complementary ^{31}P NMR titration experiments quantified a dynamic equilibrium interaction nature between DIPEA and **2a** during the EDA complex maturation with the gradual upfield shift of **2a**'s phosphorus signal (δ = 22.18→22.68 ppm) (Figure 5e).[31] Following radical inhibition studies provided decisive mechanistic evidence: introducing 4 equiv. 2,2,6,6-tetramethyl-1-piperinedinyloxy (TEMPO)—a potent radical scavenger—completely suppressed both **2a** and **2am** transformations (Figure S3). Direct spin-trapping electron spin resonance (ESR) studies under standard conditions captured distinct radical signatures: irradiation of **2a**/DIPEA with *C*-phenyl-*N*-*tert*-butylnitrone (PBN) generated a sextet spectrum (g = 2.0088, A_N = 0.86 mT, A_H = 1.49 mT) diagnostic of aryl radicals (Figure 5b),[41] while **2am**/DIPEA/5,5-dimethyl-1-pyrroline *N*-oxide (DMPO) systems produced alkyl radical adducts (g = 2.0093, A_N = 1.42 mT, A_H = 1.96 mT) (Figure 5c).[41] Control experiments confirmed photochemical specificity—no spin adducts emerged without light or phosphonium substrates.

To gain deep insights into the origin of chemoselectivity in P─C bond homolysis, we selected two representative substrates, **2a** and **2au**, for DFT calculations of the changes in Gibbs free energy during different bond cleavages. As delineated in Figure 5d, the radical intermediate **IM1** undergoes divergent homolysis pathways, wherein P–phenyl bond cleavage (**Path 1**) exhibits a lower energy change than P–(4-OMe-phenyl) scission (**Path 2**) (ΔG = 3.6 vs. 4.2 kcal mol^{-1}). This energy difference quantitatively validates enhanced bond strength between electron-rich aryl groups and the phosphorus center relative to unsubstituted phenyl systems. Experimentally observed high selectivity for **Path 1** (**3a**:triphenylphosphine = 20:1, Figure S10) further corroborates P─C bond dissociation energy (BDE) as the determinant of chemoselectivity. Complementary analysis of **IM2** reveals an amplified energy gap: P─C(sp^3) cleavage (**Path 3**, ΔG_3 = -16.7 kcal mol^{-1}) is kinetically favored over P─C(sp^2) homolysis (**Path 4**, ΔG_4 = 3.9 kcal mol^{-1}) by 20.6 kcal mol^{-1}, consistent with the experimentally results (**5i**:trialkylphosphine = 20:1, Figure S17). This pronounced contrast mechanistically substantiates our hypothesis: π-conjugated systems exert superior electronic donation to P-centered radicals versus σ-bonds, thereby elevating P─C(sp^2) BDE and establishing the selectivity hierarchy of electron-rich aryl > phenyl > alkyl.

Based on comprehensive mechanistic evidence and our research experience,[37–40] a plausible reaction pathway and the origin of the chemoselectivity were proposed (Figure 5f). The reaction initiates with dynamic formation of a photoactive EDA complex containing a pentacoordinated-phosphorane center between phosphonium salt **2** and

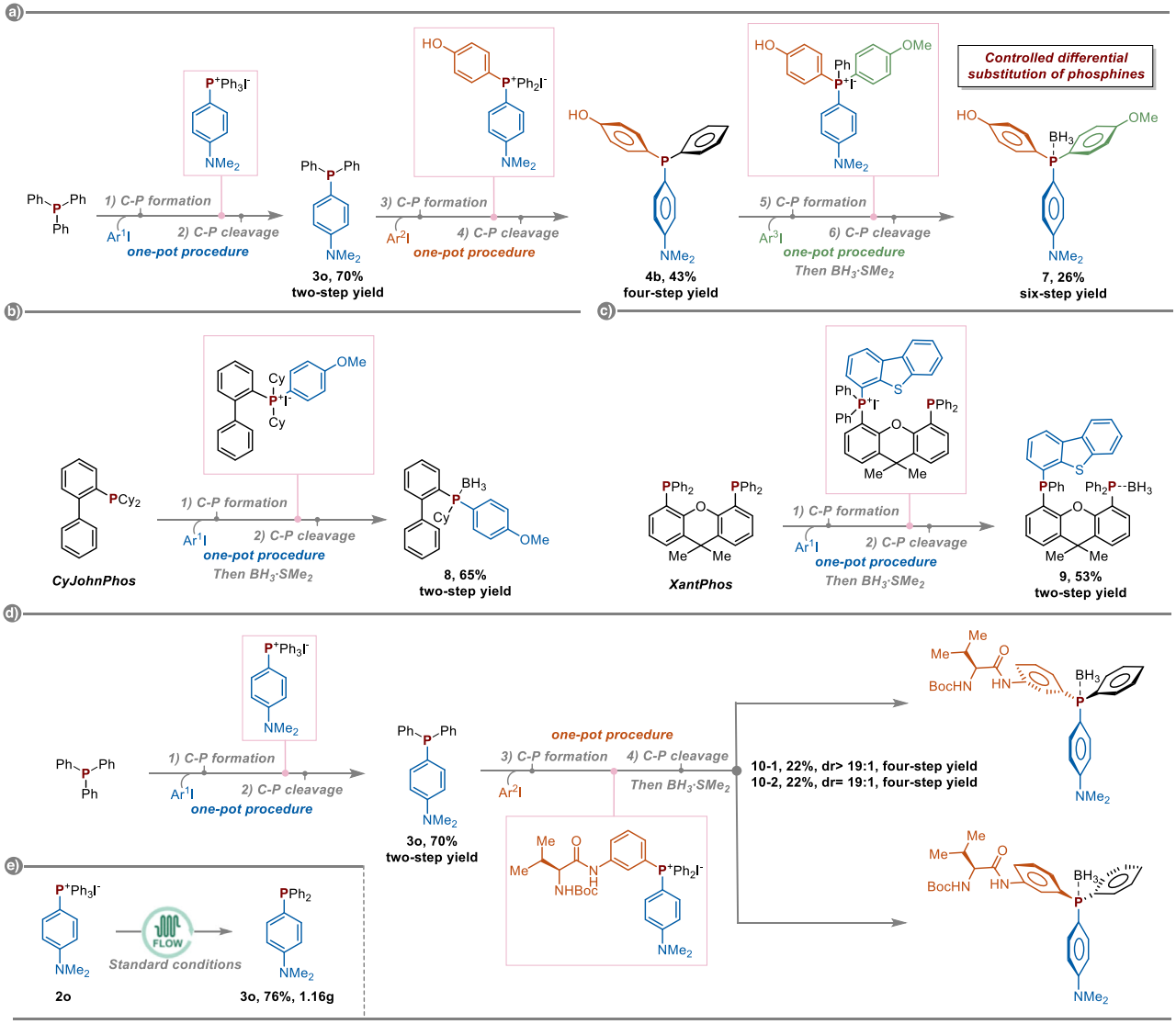

Figure 4. Synthetic applications. a) Synthesis of tri-controllable-differentially-substituted phosphine by three consecutive aryl substitutions. b) Post-modification of CyJohnphos. c) Post-modification of Xantphos. d) Synthesis of single-configuration tri-differentially-substituted phosphine. e) Gram scale synthesis in flow.

DIPEA.[39–40] Upon 405 nm irradiation, this complex reaches its excited state and consequently undergoes an intramolecular SET, generating a P-centered radical intermediate (**IM**) and a DIPEA radical cation (DIPEA$^{\bullet+}$).[42,43] Chemoselective homolytic scission of one of the four P─C bonds is achieved, liberating the trivalent phosphine product **3** alongside a carbon-centered radical ($R^{1\bullet}$). The chemoselectivity originates from the electronic modulation of P─C bond stability in the P radical intermediate. As an electron-deficient center, the phosphorus radical prefers to accept electrons from adjacent substituents. Electron-rich aryl groups (e.g., electron-donating-group *para*-substituted ones) effectively donate the wealthy electron density of the aromatic system into the radical core and thereby strengthen the corresponding P─C bond. Consequently, electron-deficient aryl groups exhibit preferential cleavage over both phenyl and electron-rich aryl substituents. In contrast, alkyl substituents lacking π-systems can only participate in weaker electron contribution, rendering their P─C bonds more susceptible to homolytic cleavage. This electronic differentiation aligns with experimental observations: electron-rich aryl groups demonstrate higher retention rates compared to alkyl or electron-deficient aryl substituents, and alkyl groups are the most preferential leaving ones. Finally, the procedure concludes through hydrogen atom transfer (HAT) between DIPEA$^{\bullet+}$ and the carbon-centered radical ($R^{1\bullet}$), yielding the hydrocarbon byproduct and oxidized DIPEA derivatives.

Conclusion

We have developed a photochemical strategy that overcomes long-standing challenges in phosphine diversification through chemoselective P─C bond cleavage. The EDA

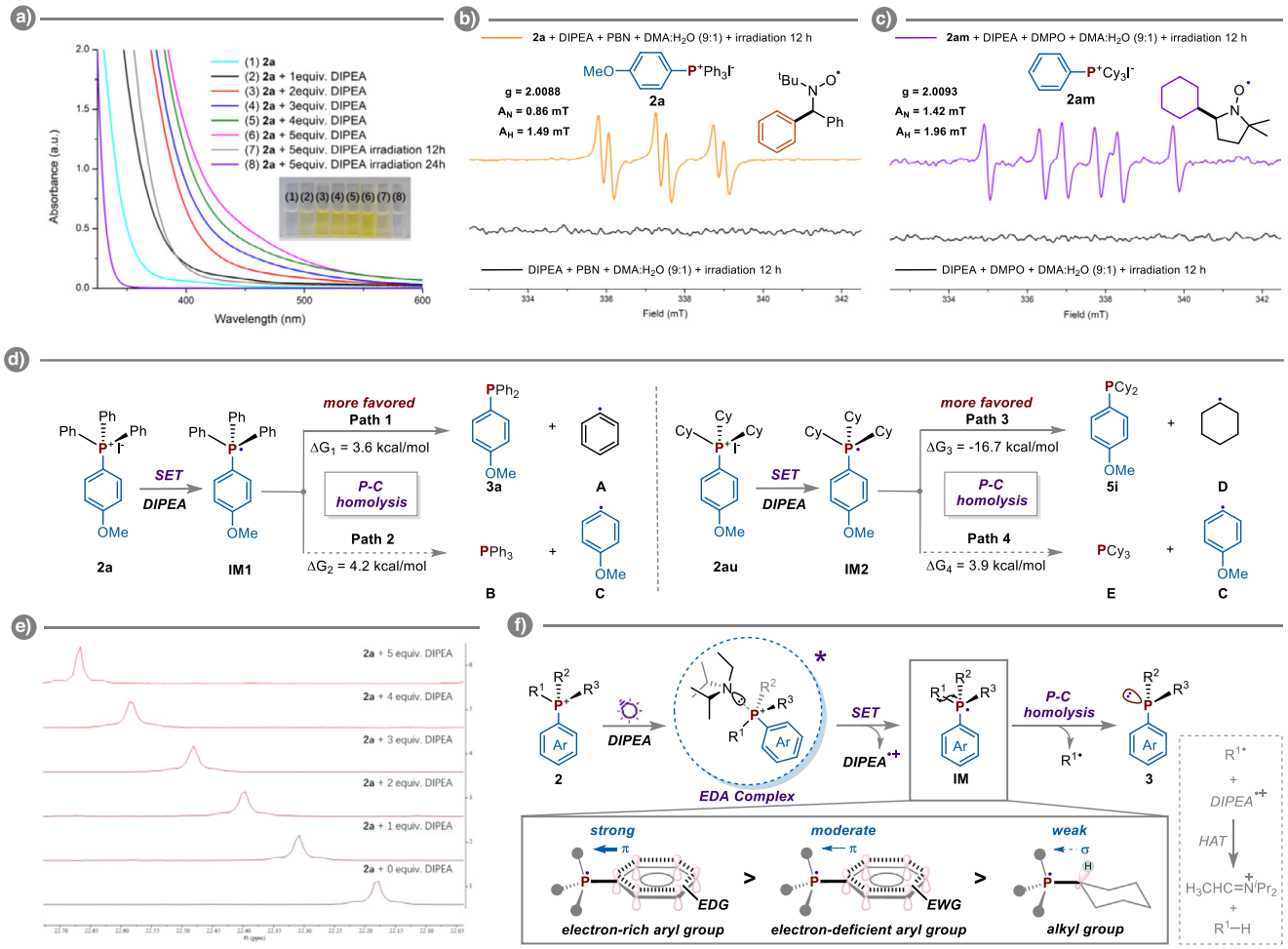

Figure 5. Mechanistic studies. a) UV-visible absorption spectroscopy experiments. b) Aryl radical detecting experiment of **2a**. c) Alkyl radical detecting experiment of **2am**. d) Computational studies of the chemoselectivity of P—C bond homolysis. e) ^{31}P NMR titration experiment. f) Proposed mechanism.

complex-mediated process enables three consecutive and customizable aryl substitutions under mild, metal-free conditions, achieving unprecedented control over phosphine architectures. Key advances include mild and metal-free procedures, broad scope, tolerance of sensitive functionalities (-NH_2, -OH) without protection, and scale-up synthesis in flow. The dynamic pentacoordinated-phosphorane EDA-complex assembling nature and the radical-mediated pathway were rigorously verified through ESR trapping experiments and spectroscopic studies. The observed chemoselectivity was proposed to root in electronic modulation of P—C bond strengths. By enabling direct modification of commercial ligands (CyJohnPhos, XantPhos)/anti-inflammatory drugs and construction of chiral P-stereogenic centers (dr > 20:1), this methodology bridges synthetic chemistry with practical applications in catalysis and pharmaceutical sciences. The elimination of transition metal residues addresses critical purity challenges, positioning this approach as an indispensable tool for next-generation ligand design and functional molecule development.

Acknowledgements

The authors acknowledge the assistance of Professor Shengyang Tao and Professor Lijing Zhang in the School of Chemistry at Dalian University of Technology (DUT) for their great help in flow chemistry. The authors acknowledge the assistance of Dr. Huihui Wan in DUT Instrumental Analysis Center for her great help in high-resolution mass spectrometry (HRMS) analysis.

Conflict of Interests

The authors declare no conflict of interest.

Data Availability Statement

The data that support the findings of this study are available in the Supporting information of this article.

Keywords: EDA complex • P—C cleavage • Phosphines • Photocatalysis

[1] H. Tian, J. Wang, G. Lai, Y. Dou, J. Gao, Z. Duan, X. Feng, Q. Wu, X. He, L. Yao, L. Zeng, Y. Liu, X. Yang, J. Zhao, S. Zhuang, J. Shi, G. Qu, X.-F. Yu, P. K. Chu, G. Jiang, *Chem. Soc. Rev.* **2023**, *52*, 5388–5484.

[2] J. B. Rodriguez, C. Gallo-Rodriguez, *ChemMedChem* **2019**, *14*, 190–216.

[3] J. H. Beigel, K. M. Tomashek, L. E. Dodd, A. K. Mehta, B. S. Zingman, A. C. Kalil, E. Hohmann, H. Y. Chu, A. Luetkemeyer, S. Kline, D. L. Castilla, R. W. Finberg, K. Dierberg, V. Tapson, L. Hsieh, T. F. Patterson, R. Paredes, D. A. Sweeney, W. R. Short, G. Touloumi, D. C. Lye, N. Ohmagari, M. Oh, G. M. Palacios, T. Benfield, G. Fätkenheuer, M. G. Kortepeter, R. L. Atmar, C. B. Creech, J. Lundgren, et al., *N. Engl. J. Med.* **2020**, *383*, 1813–1836.

[4] H. Yu, H. Yang, E. Shi, W. Tang, *Med. Drug Discovery* **2020**, *8*, 100063.

[5] P. Ma, Y. Chen, Y. Man, Q. Qi, Y. Guo, H. Wang, Z. Li, P. Chang, C. Qu, C. Han, H. Xu, *Angew. Chem. Int. Ed.* **2024**, *136*, e202316479.

[6] R. Martin, S. L. Buchwald, *Acc. Chem. Res.* **2008**, *41*, 1461–1473.

[7] D. S. Surry, S. L. Buchwald, *Angew. Chem. Int. Ed.* **2008**, *47*, 6338–6361.

[8] T. Gensch, G. dos Passos Gomes, P. Friederich, E. Peters, T. Gaudin, R. Pollice, K. Jorner, A. Nigam, M. Lindner-D'Addario, M. S. Sigman, A. Aspuru-Guzik, *J. Am. Chem. Soc.* **2022**, *144*, 1205–1217.

[9] H. Guo, Y. C. Fan, Z. Sun, Y. Wu, O. Kwon, *Chem. Rev.* **2018**, *118*, 10049–10293.

[10] J. Hou, J. H. Xie, Q.-L. Zhou, *Angew. Chem. Int. Ed.* **2015**, *54*, 6302–6305.

[11] B. Lin, T. Yang, D. Zhang, Y. Zhou, L. Wu, J. Qiu, G. Q. Chen, C. M. Che, X. Zhang, *Angew. Chem. Int. Ed.* **2022**, *61*, e202201739.

[12] P. Mei, Z. Ma, Y. Chen, Y. Wu, W. Hao, Q.-H. Fan, W.-X. Zhang, *Chem. Soc. Rev.* **2024**, *53*, 6735–6778.

[13] K. Dong, Y. Li, Z. Wang, K. Ding, *Angew. Chem. Int. Ed.* **2013**, *52*, 14191–14195.

[14] S. H. Newman-Stonebraker, S. R. Smith, J. E. Borowski, E. Peters, T. Gensch, H. C. Johnson, M. S. Sigman, A. G. Doyle, *Science* **2021**, *374*, 301–308.

[15] J. Yang, J. Liu, H. Neumann, R. Franke, R. Jackstell, M. Beller, *Science* **2019**, *366*, 1514–1517.

[16] C. Guo, D.-W. Sun, S. Yang, S.-J. Mao, X.-H. Xu, S.-F. Zhu, Q.-L. Zhou, *J. Am. Chem. Soc.* **2015**, *137*, 90–93.

[17] M. Murata, S. L. Buchwald, *Tetrahedron* **2004**, *60*, 7397–7403.

[18] D. V. Allen, D. Venkataraman, *J. Org. Chem.* **2003**, *68*, 4590–4593.

[19] W.-Q. Wu, Q. Peng, D.-X. Dong, X.-L. Hou, Y.-D. Wu, *J. Am. Chem. Soc.* **2008**, *130*, 9717–9725.

[20] S. E. Vaillard, C. Mück-Lichtenfeld, S. Grimme, A. Studer, *Angew. Chem. Int. Ed.* **2007**, *46*, 6533–6536.

[21] R. Köster, Y. Morita, *Angew. Chem.* **1965**, *77*, 589–590.

[22] A. J. Stepen, M. Bursch, S. Grimme, D. W. Stephan, J. Paradies, *Angew. Chem. Int. Ed.* **2018**, *57*, 15253–15256.

[23] Y. Li, L.-Q. Lu, S. Das, S. Pisiewicz, K. Junge, M. Beller, *J. Am. Chem. Soc.* **2012**, *134*, 18325–18329.

[24] Y. Li, S. Das, S. Zhou, K. Junge, M. Beller, *J. Am. Chem. Soc.* **2012**, *134*, 9727–9732.

[25] Z. Yang, C. Shen, K. Dong, *Chin. J. Chem.* **2022**, *40*, 2734–2740.

[26] C. Wang, Y.-H. Dai, Z. Wang, B. Lu, W. Cao, J. Zhao, G. Mei, Q. Yang, J. Guo, W.-L. Duan, *J. Am. Chem. Soc.* **2024**, *146*, 27843–27851.

[27] Z. Lian, B. N. Bhawal, P. Yu, B. Morandi, *Science* **2017**, *356*, 1059–1063.

[28] S. Roediger, S. U. Leutenegger, B. Morandi, *Chem. Sci.* **2022**, *13*, 7914–7919.

[29] M. Lei, X. Chen, Y. Wang, L. Zhang, H. Zhu, Z. Wang, *Org. Lett.* **2022**, *24*, 2868–2872.

[30] Y. H. Lee, B. Morandi, *Coord. Chem. Rev.* **2019**, *386*, 96–118.

[31] Q. Liu, B. B. Zhang, H. Sheng, S. Qiao, Z. X. Wang, X. Y. Chen, *Angew. Chem. Int. Ed.* **2023**, *62*, e202305088.

[32] Q. Liu, Y. Lu, H. Sheng, C. S. Zhang, X. D. Su, Z. X. Wang, X. Y. Chen, *Angew. Chem. Int. Ed.* **2021**, *60*, 25477–25484.

[33] S. Roediger, E. L.e Saux, P. Boehm, B. Morandi, *Nature* **2024**, *636*, 108–114.

[34] F. Y. Kwong, C. W. Lai, M. Yu, Y. Tian, K. S. Chan, *Tetrahedron* **2003**, *59*, 10295–10305.

[35] F. Y. Kwong, K. S. Chan, *Organometallics* **2000**, *19*, 2058–2060.

[36] Z. Gan, J. Chen, H. Wang, Z. Xue, Z. Chen, Y. Zhang, L. Wang, H. Zi, S. Liu, L. Shi, Y. Jin, *Org. Lett.* **2024**, *26*, 7751–7756.

[37] Z. Xu, Z. Chen, S. Liu, J. Gao, J. Lei, M. Li, Y. Zhang, Z. Gan, L. Yu, S.-X. Liu, Y. Jin, *Green Chem.* **2025**, *27*, 8126–8132.

[38] R. Cui, Q. Liao, Y. Zhao, L. Wang, Y. Zhang, S. Liu, Z. Gan, Y. Chen, Y. Shi, L. Shi, M. Li, Y. Jin, *Org. Lett.* **2024**, *26*, 8222–8227.

[39] H. Fu, Z.-L. Li, Y.-F. Zhao, G.-Z. Tu, *J. Am. Chem. Soc.* **1999**, *121*, 291–295.

[40] H. Fu, J.-H. Xu, R.-J. Wang, Z.-Z. Chen, G.-Z. Tu, Q.-Z. Wang, Y.-F. Zhao, *Phosphorus, Sulfur, and Silicon* **2003**, *178*, 1963–1971.

[41] G. R. Buettner, *Free Radical Biol. Med.* **1987**, *3*, 259–303.

[42] B. Lu, Z. Zhang, M. Jiang, D. Liang, Z. W. He, F. S. Bao, W. J. Xiao, J. R. Chen, *Angew. Chem. Int. Ed.* **2023**, *62*, e202309460.

[43] X. Dang, Z. Li, J. Shang, C. Zhang, C. Wang, Z. Xu, *Angew. Chem. Int. Ed.* **2024**, *136*, e202400494.

Manuscript received: April 30, 2025
Revised manuscript received: July 08, 2025
Accepted manuscript online: July 08, 2025
Version of record online: July 17, 2025